Bull. Mater. Sci. (2021) 44:238
https://doi.org/10.1007/s12034-021-02509-z

Turbulent fluid flow-assisted rapid electrodeposition of Zn–Ni γ-phase from modified Watt's type bath by addition of saccharin

VAHID ABBASI-CHIANEH* and FERYAL SHOKRANI
Department of Materials Engineering, Urmia University of Technology, Urmia 57166-93187, Iran
*Author for correspondence (v.abbasi@uut.ac.ir; vahid61abbasi@gmail.com)

MS received 19 March 2021; accepted 7 June 2021

Abstract. Rapid electrodeposition is economically a valuable way that has led to the invention of different methods. In this study, rapid Zn–Ni γ-phase electrodeposition from modified Watt's bath containing zinc ions was investigated. A high current density was applied in assistance with the turbulent fluid flow as a simple technique for rapid electrodeposition, and the influence of saccharin amount was investigated on microstructure and corrosion resistance of rapid electrodeposited films. Rapid electrodeposition led to the formation of a preferred texture orientation of (600) and a small crystallite colony size. Structural changes and variation in the composition of rapid electrodeposited γ-phase resulted in improved corrosion resistance. The addition of saccharin into the electrolyte altered the preferred crystal texture to (300) and increased the crystallite colony size, accompanied by changing diamond-like morphology to the faceted surface and inhibited formation of microcracks that were detected in rapid electrodeposited films.

Keywords. Rapid electrodeposition; γ-phase; Zn–Ni; saccharin additive; corrosion.

1. Introduction

Zinc coatings have been widely employed for the protection of steel parts from corrosion, due to low melting point and low zinc cost [1]. These sacrificial coatings remain effective on steel even after being worn or cracked and protect the substrate galvanically. However, the high electrode potential of zinc with respect to steel results in rapid corrosion of zinc coats. This process could result in reduced performance of the coats [2,3]. Substitution of pure zinc with Zn–Ni alloys has been investigated extensively due to their improved corrosion resistance and better physical properties than pure zinc [3,4]. Co-electrodeposition of nickel and zinc from aqueous solutions materializes while the nickel deposition is strongly inhibited, and the zinc deposition is induced by the coincident presence of Zn^{2+} and Ni^{2+} ions [5,6].

Steel parts with electrodeposited Zn–Ni alloys are employed in different applications, such as aeronautic, automobile, oil and gas industries [5–7]. The amount of nickel should be determined according to the application and required properties of coated parts, which strongly affects formability, paintability, weldability and corrosion resistance as important functional factors [5–7]. According to phase diagram and recent studies of Ni–Zn alloys, there are five well-known phases for Zn–Ni alloys, which are α, η, β1, γ and δ. α is a nickel-rich solid solution that contains less than 30 wt% zinc, η is a zinc-rich phase with less than 1% nickel, β1 exists approximately between 48 wt% Zn and 55 wt% Zn, γ-phase exists from 72 wt% Zn to 87 wt% Zn known as Ni_5Zn_{21} and δ is a stoichiometric compound phase with Ni_3Zn_{22} composition [2,8,9]. However, differences between alloy composition of the phases for electrodeposited and thermally processed alloys have been reported. In some studies, the β1-phase was not detected, and the composition range for deposited γ-phase could be expanded [10,11]. Researches have illustrated that enhanced brightness and uniformity along with γ-phase formation could result in improved corrosion resistance of Zn–Ni alloy coats [12,13].

Furthermore, new techniques and approaches, including techniques for increased current density and using additives, could result in lower costs, higher efficiency, and improved physical and mechanical properties of coats [14–20]. Different methods such as laser-assisted methods, jet electrodeposition (JED), and utilizing high-speed turbulent flow (HSTF) have been considered as increased current density methods (rapid electrodeposition methods) [17]. Among these techniques, HSTF is a simple and less limited method. HSTF is based on fast electrolyte flow between the anode and the cathode. In addition to simplicity and low degree of limitation, HSTF has the advantages of being applicable on a large-scale, less time-consuming, and high quality and uniformity of applied coats [15]. In conventional electrodeposition, the current density is limited by depletion of cations and reduction of hydrogen ions instead of cations

Published online: 30 August 2021

near the cathode. Reduced hydrogen ions could lead to burnt deposits in conventional electrodeposition, while the HSTF process could be used with a much higher current density. Elimination of hydrogen in the HSTF method is the critical point that occurs due to reduction of the well-known diffusion layer situated between the cathode and bulk of the solution by mass transport phenomena due to increased velocity of the electrolyte flow at the cathode surface [17]. In the case of zinc–nickel deposition, utilizing the HSTF method could be very beneficial due to the anomalous behaviour of Zn–Ni codeposition. Anomalous behaviour of electrodeposition of zinc in zinc–nickel coatings is reported and analysed in many studies [21,22]. Zn–Ni electrodeposition is classified as an anomalous codeposition through which a less noble zinc metal (active) is deposited, and its percentage in the deposition is more than the bath. It is confirmed that the anomalous behaviour is attributed to the local increase in pH as a result of hydrogen evolution [23]. As the HSTF method reduces the diffusion layer and hydrogen evolution, it seems that it could be beneficial in codeposition of Zn–Ni layers.

For the improvement of HSTF, using additives could be useful as employed in conventional electrodeposition [8,16,19]. The saccharin effect has been studied extensively as an additive for electrodeposition.

The addition of saccharin to the electrolytes causes structural, morphological and compositional changes [8,16,24,25]. It has been confirmed that the addition of saccharin to the electrolyte could decrease the surface roughness and the size of crystallites in electrodeposited Zn–Ni alloy films [8]. Moreover, it has been reported that (111), (200) double fibre mode texture could be attained instead of (200) mode on adding saccharin to the nickel electrodeposition bath [26]. Researches indicate that saccharin has two different roles in the electrodeposition process: (1) the overpotential is modified due to compositional change in the Helmholtz layer, and (2) active growth sites are occupied by adsorbed saccharin anions on the cathode and act as a barrier layer for ions (inhibition of ion reduction) and therefore inhibit the growth on the cathode. The barrier layer may be created by chemisorption or electrostatic interaction between negatively charged cathode and unsaturated benzene ring in saccharin. These two roles of saccharin could change the Ni content in electrodeposited films leading to structural and phase changes [8,19,27]. However, the effect of saccharin addition on the structure of rapid electrodeposited Zn–Ni alloy coatings needs to be further examined for different functional properties.

The aim of this research is based on rapid electrodeposition of Zn–Ni γ-phase using the HSTF method and investigating the effect of saccharin additive on microstructure and corrosion resistance of Zn–Ni alloy coats.

2. Materials and methods

Mild steel plates were used as substrates that were positioned vertically in the electrodeposition chamber. The sizes of the nickel plate as the anode and the steel substrate were $100 \times 10 \times 2$ and $10 \times 10 \times 2$ mm^3, respectively. The substrates were degreased in 1 molar NaOH solution at 400°C for 1 min, followed by rinsing with distilled water. Degreased substrates were activated by 20% HCl solution at room temperature for 1 min and were thoroughly washed with distilled water immediately after activation, before placing it in the electrodeposition chamber.

The composition of the electrolyte is given in table 1, which is based on Watt's bath solution. The solution is modified with zinc sulphate as a supply for zinc ions needed for Zn–Ni alloy electrodeposition and sodium dodecyl sulphate as a brightening agent. As acidic and alkaline baths have been studied extensively, this bath is selected based on low thickness distribution and minimal alloy changes in acidic baths. Moreover, blocking effect of boric acid on hydrogen release and keeping the pH in the bath as a buffer which is necessary for rapid electrodeposition of anomalous Zn–Ni electrodeposition, are some of the reasons to use Watt's type bath [28].

The distance between the anode and the cathode was fixed to 2 mm, and the chamber's cross-sectional area was 20 mm^2. The flow rate of the electrolyte between the anode and the cathode was controlled to have a turbulent flow. Selecting the electrolyte velocity is based on achieving Reynold's number of more than 4000, resulting in the transition of laminar to turbulent flow regime. Reynold's number is calculated based on equation (1):

$$\mathrm{Re} = \rho DV/\eta \tag{1}$$

where D is the characteristic length, V the average velocity, ρ the density, and η the electrolyte's viscosity.

The schematic of the HSTF equipment is shown in figure 1, which contains an electrodeposition chamber, a

Table 1. Composition of the electrolyte.

	Zinc sulphate	Sodium dodecyl sulphate	Boric acid	Nickel chloride	Nickel sulphate
Composition of the electrolyte (g l^{-1})	90	0.25	45	45	170

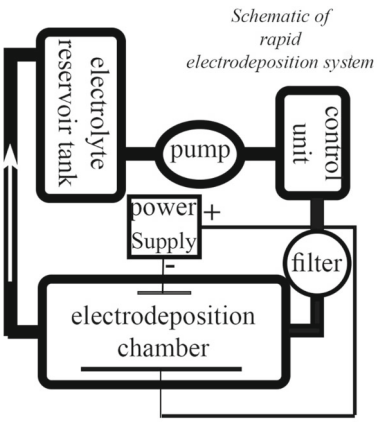

Figure 1. Schematic of the HSTF electrodeposition equipment.

Table 2. Electrodeposition variable parameters for different samples.

Sample no.	Current density (A dm^{-2})	Time (min)	Saccharin (g l^{-1})
1	4	20	0
2	4	20	3
3	4	20	5
4	4	20	7
5	0.4	2	0
6	0.4	2	3
7	0.4	2	5
8	0.4	2	7

reservoir of electrolyte, a pump, a filtration system, a flow rate control unit and a DC power supply.

Electrodeposition was carried out using 3 litres of electrolyte in the reservoir tank, maintaining the temperature at 50°C, applying different current densities (4–100 A dm^{-2}), and 3–7 g l^{-1} of saccharin as an additive. The pH has been adjusted to 4 by adding one molar NaOH solution and sulphuric acid.

Different samples were electrodeposited for 2 min with an electrolyte velocity of 2.7 m s^{-1} to find current density of Zn–Ni alloy with the HSTF method.

Visual examination was used to determine the maximum current density for rapid electrodeposition for suitable coating appearance. The samples were coated at 40 A dm^{-2} for the rapid electrodeposition method and 4 A dm^{-2} for the conventional method. Different electrodeposition conditions for further investigations are listed in table 2.

Crystal structures of the electrodeposited alloys were examined using D8 Advance Brucker diffractometer using Cu kα radiation in the angular range of 45–100° with step size and delay time of 0.05° and 1 s, respectively. Surface morphology and composition analysis were determined utilizing MIRA III TESCAN scanning electron microscopy equipped with an energy dispersive spectrometer. Electrodeposited alloys' hardness was determined using an MDPEL-M400 microhardness tester under 50 g load force and 10 s indentation time. The corrosion resistance of the samples with 3.5 wt% NaCl solution in distilled water was examined with potentiodynamic polarization measurement utilizing the Ivium vertex instrument.

Table 3. Electrolyte composition determined by AAS.

	Zinc ions	Nickel ions	Ni/(Ni + Zn) wt%
Measured ion (mg l^{-1})	20,491	52,206	72

3. Results and discussion

3.1 *Determining the rapid electrodeposition current density utilizing the HSTF method*

Table 3 indicates the nickel and zinc ion concentrations in the electrolyte that were determined using atomic absorption spectroscopy (AAS). According to other researches, the ratio of Ni ions to total metal ions (Ni^{2+}/(Ni^{2+}+Zn^{2+}) wt%) plays an important role on the Ni content of deposited films. The ratio of 72 wt% in table 3 indicates that the Zn–Ni alloy coatings crystallize in γ-phase structure containing 10–20% Ni atoms because of anomalous Zn–Ni electrodeposition [6,29,30].

Optical images of electrodeposited alloy coatings at different current densities are presented in figure 2 for visual comparison. As illustrated in figure 2, the coated sample under a current density of 80 A dm^{-2} is completely blackened due to high current density. Decreasing the current density resulted in an improved appearance of electrodeposited films. However, reducing the current density to 50 A dm^{-2} resulted in an acceptable appearance in the middle of the sample, while the rabbit ear defect was evident due to the high current density at the sample edges. By reducing the current density to 40 A dm^{-2}, the sample quality seems to be acceptable. Furthermore, sample D with 7 g l^{-1} of saccharin in the electrolyte resulted in a shiny and reflective appearance.

The current density of 40 A dm^{-2} is approximately ten times more than conventional current densities (0.03–0.05 A cm^{-2}) for the zinc alloy coatings. Thus, using a high current density of 40 A dm^{-2} accompanied with the electrolyte's high turbulent flow supports the rapid electrodeposition of Zn–Ni alloy without visual defects, such as scaling or burned layer.

Further investigations were based on rapid electrodeposition of Zn–Ni alloys at current density of 40 A dm^{-2}

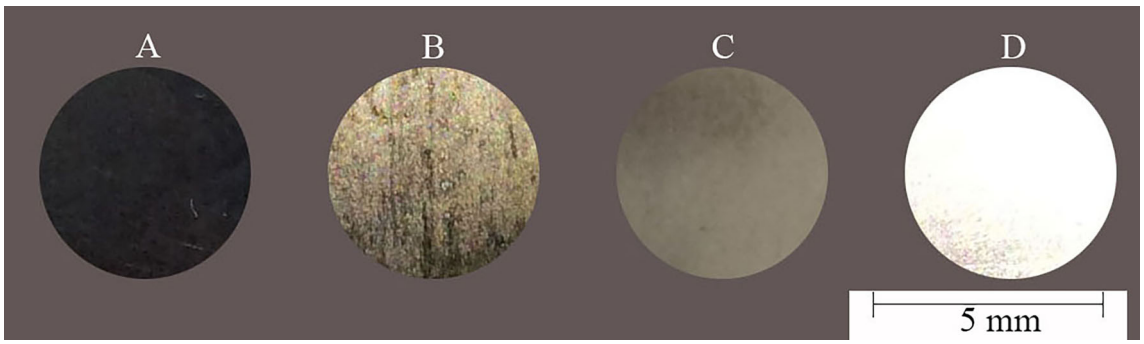

Figure 2. Optical image of sample surfaces; electrodeposited at different current densities of: (**A**) 80 A dm^{-2}, (**B**) 60 A dm^{-2}, (**C**) 40 A dm^{-2} and (**D**) 40 A dm^{-2} with 7 g l^{-1} of saccharin in the electrolyte.

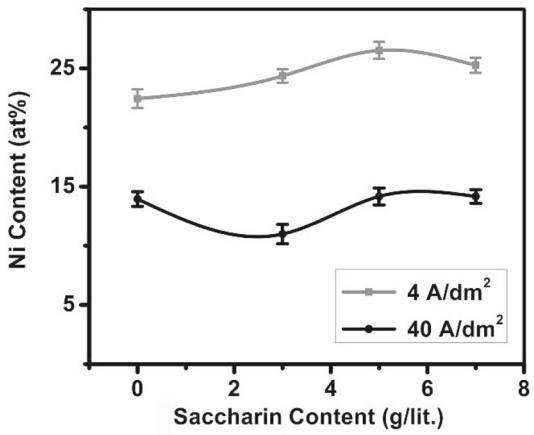

Figure 3. Effect of saccharin addition into the electrolyte on nickel content of electrodeposited alloy films at current densities of 4 and 40 A dm^{-2}.

compared with alloys that were electrodeposited at conventional current densities of 4 A dm^{-2}.

3.2 *Chemical and structural analyses*

Nickel contents of electrodeposited films were analysed using energy dispersive spectroscopy (EDS). The nickel contents of the films as a function of saccharin amount in the electrolyte are plotted in figure 3 for applied current densities of 4 and 40 A dm^{-2}.

According to figure 3, the nickel contents of alloys that were electrodeposited at 40 A dm^{-2} are lower than that of alloys generated at 4 A dm^{-2}, for all saccharin values. The high nickel content of generated films at 4 A dm^{-2} compared with films generated at 40 A dm^{-2} indicates that nickel's electrodeposition is diffusion-controlled. In contrast, the raised current density led to the increased content of zinc in the electrodeposited films that is due to a high level of overpotential and activation-controlled mechanism for zinc electrodeposition.

The addition of saccharin agent into the electrolyte resulted in different behaviours of rapid and conventional electrodeposition methods. Saccharin addition to the electrolyte for electrodeposition at 4 A dm^{-2} resulted in the raised nickel content in the films. However, at 40 A dm^{-2} of current density, the nickel content in the films initially decreased by saccharin addition. In contrast, further addition of saccharin increased the nickel content of the films, similar to the indicated trend of electrodeposition at 4 A dm^{-2}. The effect of saccharin addition on nickel content of rapid and conventional electrodeposited films could be differed due to different nucleation and growth mechanisms. However, adding saccharin into the electrolyte inhibits zinc ions electrodeposition with conventional electrodeposition. In addition, a similar trend was detected for rapid electrodeposition at higher amounts of saccharin (5–7 g l^{-1}). However, compositional changes may lead to different phase formations according to Zn–Ni phase diagram that should be investigated.

X-ray diffraction (XRD) patterns are studied to investigate differences between Zn–Ni phases with conventional and rapid electrodeposition methods. Figure 4 shows XRD patterns for the electrodeposited films at different current densities and different saccharin contents.

The XRD pattern of the sample that was electrodeposited with the conventional method (figure 4a) revealed that the γ-phase of Zn–Ni alloy had been crystallized. Considering the phase and chemical composition of deposited layers illustrates that the phase formation by electrodeposition do not differ with thermally processed alloys with 73–87 wt% Zn and in both cases, the γ-phase is detected. Comparing the XRD pattern of rapid electrodeposited samples with the conventional method illustrates that rapid electrodeposition resulted in preferential growth of γ-phase crystallite in ⟨600⟩ direction so that the dominant peak in the pattern (figure 4d) is (600). The presence of texture indicates that different crystallographic planes have different growth rates. In the absence of saccharin, the peak intensity of (600) raised with an increase in current density of 40 A dm^{-2}. Among five well-known growth types of polycrystals ((1) field-orientated isolated crystals type (FI), (2) basis-orientated reproduction type (BR), (3) twinning intermediate type (Z), (4) field-orientated texture type (FT) and (5)

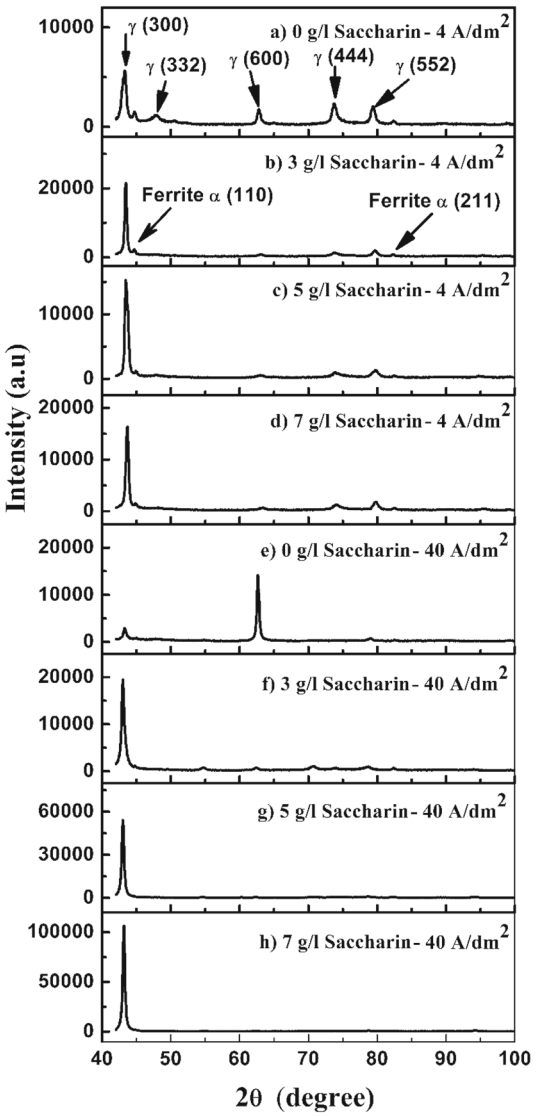

Figure 4. XRD diffraction patterns of coated films at electrodeposition current densities of (**a–d**) 4 A dm^{-2} and (**e–h**) 40 A dm^{-2} and saccharin contents of (**a** and **e**) 0 g l^{-1}, (**b** and **f**) 3 g l^{-1}, (**c** and **g**) 5 g l^{-1} and (**d** and **h**) 7 g l^{-1} in the electrolyte.

unoriented dispersion type (UD)), it is assumed that type 4 of growth mechanism i.e., field-oriented texture prevails along ⟨600⟩ direction [31,32]. However, the inhibition mechanism of adsorbed ions and the high current density that leads to overpotentials at the cathode surface need to be investigated in more detail to illustrate the inhibition and easy growth direction mechanisms.

The XRD patterns also demonstrate that the addition of saccharin to the electrolyte altered the preferred growth direction, so that the intensity of the (300) peak raised significantly by increasing the saccharin amount. As a result, it could be considered that the addition of saccharin could defeat the effect of current density on the texture change. Moreover, small peak shifts are detected based on raised saccharin amount in the electrolyte. Increasing the saccharin content led to the peak shift to higher diffraction angles in conventionally electrodeposited films. In the rapid electrodeposition method, adding 3 g l^{-1} of saccharin shifted the (300) peak to the lower angles. In contrast, increasing the saccharin content to higher levels, i.e., more than 3 g l^{-1}, resulted in a peak shift to higher angles. The peak shift might be due to the compositional changes in electrodeposited layers as well as the affected residual stresses induced by the addition of saccharin to the electrolyte.

Figures 3 and 4 conclude that the preferred growth direction of ⟨300⟩ that was induced by saccharin in rapid electrodeposited films resulted in decreased nickel adsorption as compared to ⟨600⟩ growth direction. Saccharin values more than 3 g l^{-1} in the conventional and rapid electrodeposition methods resulted in a nearly similar nickel content variation trend in films against the saccharin content in electrolyte due to identical achieved texture modes.

The surface morphology of electrodeposited Zn–Ni alloys was investigated using SEM, as shown in figure 5. Adding 3 g l^{-1} of saccharin into the electrolyte changed the diamond-like crystallite morphology to a globular one in the conventionally electrodeposited films as shown in figure 5. Further increasing the saccharin to 7 g l^{-1} led to a facet surface morphology. Figure 5 also illustrates that rapid electrodeposition resulted in fine grains of crystallites on the surface. Moreover, adding saccharin to the electrolyte resulted in completely faceted surface morphology in rapid electrodeposited films. However, large cracks were observed in rapid electrodeposited layers that were eliminated by adding the saccharin into the electrolyte. According to XRD results, it could be concluded that these cracks could be a result of residual stresses (peak shift in XRD pattern) and the formation of (600) texture in rapid electrodeposited layers. As the addition of saccharin into the electrolyte changed the texture and nickel content of electrodeposited layers, it would be difficult to determine the exact mechanism of crack elimination.

3.3 *Properties of hardness and corrosion resistance*

Microhardness and polarization tests were used to determine the effects of compositional and microstructural changes on the hardness and corrosion properties of the electrodeposited films. Microhardness values of the electrodeposited layers were plotted against the saccharin content for the conventional and rapid electrodeposited films in figure 6.

Figure 6 shows that the hardness values of the films tend to decrease utilizing the rapid electrodeposition method. The reduced hardness values due to rapid electrodeposition could have resulted from nickel depletion in the rapid electrodeposited layers. However, the difference between the hardness values of electrodeposited films in saccharin-free electrolytes was less valuable for conventional and

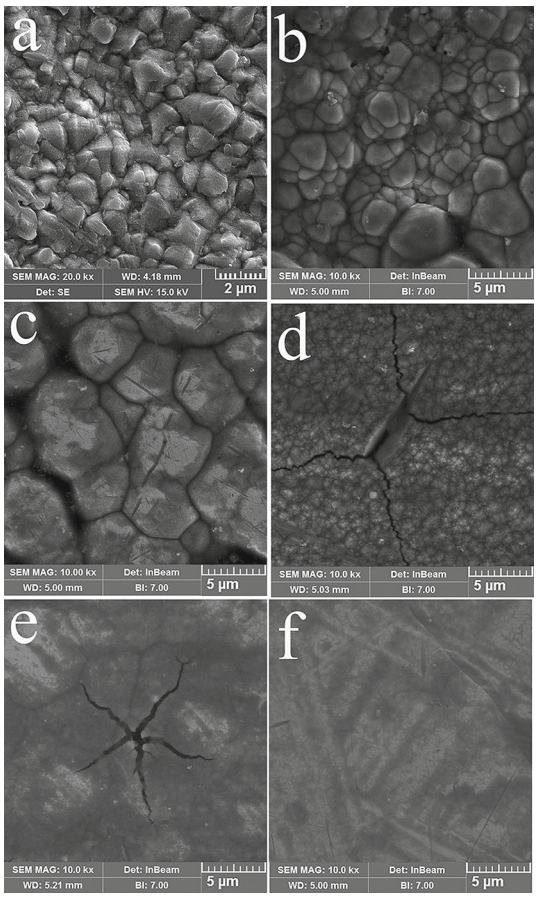

Figure 5. SEM images of electrodeposited films at 4 A dm^{-2}: (**a**) without saccharin addition, (**b**) with 3 g l^{-1} of saccharin, (**c**) with 7 g l^{-1} of saccharin and at 40 A dm^{-2}: (**d**) without saccharin addition, (**e**) with 3 g l^{-1} of saccharin, (**f**) with 7 g l^{-1} of saccharin.

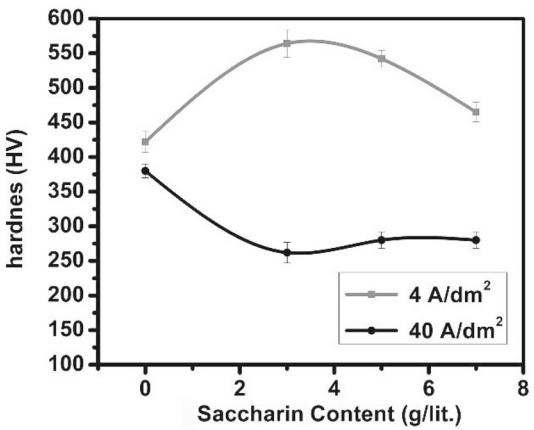

Figure 6. Microhardness value of electrodeposited films by conventional and rapid electrodeposition method against different amounts of saccharin in the electrolyte.

rapid electrodeposition methods. The (600) texture mode of the rapid electrodeposited layer in the absence of saccharin might be the reason for a small decrease in microhardness

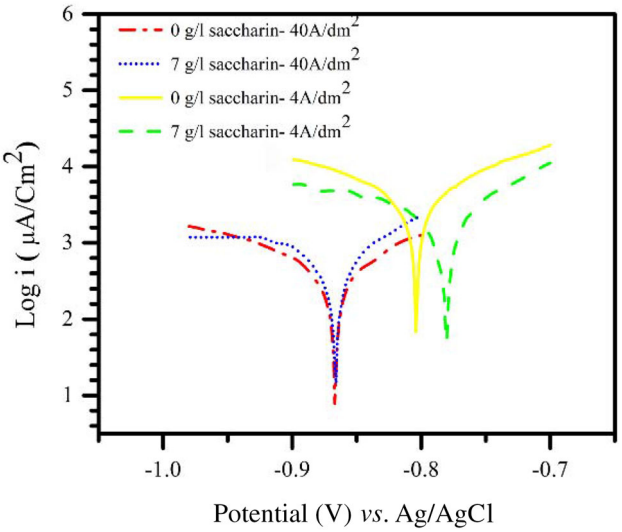

Figure 7. Potentiodynamic polarization curves in logarithmic scale.

Table 4. Polarization data for electrodeposited Zn–Ni films.

Sample	R_p (Ω cm^{-2})	J_{corr} (mA cm^{-2})	E_{corr} (V)
4 A cm^{-2}–0 g l^{-1} Saccharin	5.97	1.37	−0.8
4 A cm^{-2}–7 g l^{-1} Saccharin	9.23	0.93	−0.78
40 A cm^{-2}–0 g l^{-1} Saccharin	36.01	0.18	−0.86
40 A cm^{-2}–7 g l^{-1} Saccharin	26.49	0.26	−0.86

value in contrast with a high nickel content depletion in the films. Moreover, the addition of saccharin into the electrolyte could affect the microhardness values of the films due to three different ways: (1) formation of the (300) dominant texture orientation, (2) affecting the nickel content of electrodeposited films, and (3) stress relief due to affecting the nickel content or eliminating the hydrogen gas absorbance which is mentioned in other researches [2].

The potentiodynamic polarization curves are presented in figure 7 and are used to determine corrosion potentials and current densities of rapid and conventionally electrodeposited films by the Tafel extrapolation method that are tabulated in table 4. The E_{corr} values in table 4 reveals that all electrodeposited films are suggested as sacrificial coatings for steel due to more negative values (approximately < -0.75 V) in comparison with steel (about -0.6 V). Compared to the rapid electrodeposited films, films that were electrodeposited conventionally revealed higher corrosion current densities in contrast to nobler corrosion potentials. Lower corrosion current density of rapid electroplated films is due to the dense and compact structure together with the fine surface morphology of electrodeposited films. Moreover, it can be seen from figure 7 and

table 4 that the addition of saccharin to the electrolyte affects the corrosion current and potential of rapid and conventionally electrodeposited films in different ways. The addition of saccharin led to increased corrosion potential and reduced current density of conventionally electrodeposited films that could be concerned with the faceted growth of crystallites colonies and increased nickel content in electrodeposited films. Moreover, using saccharin in the rapid electrodeposition method resulted in an increased corrosion current density. It seems that the texture of γ-phase is so effective that despite the decreased surface roughness and the crack limitations (induced by saccharin), changing the growth direction from ⟨600⟩ to ⟨300⟩ has led to raised corrosion current densities.

Finally, it could be claimed that rapid electrodeposition of Ni–Zn γ-phase is achieved by means of the HSTF method and using saccharin additive for eliminating crack formation with acceptable properties for steel coats. However, investigating other additives and electrolyte bath compositions is helpful for preserving the generated texture mode of the rapid electrodeposited films while eliminating the cracks formed in the γ-phase due to rapid electrodeposition in the absence of saccharin.

4. Conclusion

Applying high current density during electrodeposition led to crystalline texture with dominant ⟨600⟩ growth direction of Zn–Ni γ-phase and improved the corrosion resistance properties of Zn–Ni alloy films due to dense structure and preferred texture orientation. The addition of saccharin into the electrolyte resulted in an increased amount of nickel in electrodeposited films and transformed the surface morphology from diamond-like to a faceted surface so that the samples were shiny. Moreover, the addition of saccharin into the electrolyte of the rapid electrodeposition bath changed the dominant texture direction of ⟨600⟩ that was formed due to high current densities to ⟨300⟩ direction and inhibited cracking of rapid electrodeposited films. Occupation of active growth sites by adsorbed saccharin is the main reason for changing the ⟨600⟩ field oriented texture to ⟨300⟩ direction.

References

[1] Kamnerdkhag P, Toyatornmanesub P and Rodchanarowan A 2018 *Mater. Today: Proc.* **5** 9404

[2] Tafreshi M, Allahkaram S and Farhangi H 2016 *Mater. Chem. Phys.* **183** 263

[3] Li B, Li D, Xia W and Zhang W 2018 *Appl. Surf. Sci.* **458** 665

[4] Oliveira R, Bertagnolli D, Ferreira E, da Silva L and Paula A 2018 *Surf. Coat. Technol.* **349** 874

[5] Pedroza G D, de Souza C, de Jesus M, de Andrade Lima L and Ribeiro D 2014 *Surf. Coat. Technol.* **258** 232

[6] Kwon M, Jo D-H, Cho S H, Kim H T, Park J-T and Park J M 2016 *Surf. Coat. Technol.* **288** 163

[7] Bahadormanesh B, Ghorbani M and Kordkolaei N L 2017 *Appl. Surf. Sci.* **404** 101

[8] Mosavat S, Bahrololoom M and Shariat M 2011 *Appl. Surf. Sci.* **257** 8311

[9] Okamoto H, Schlesinger M E and Mueller E M (eds) 2016 *ASM Handbook: alloy phase diagrams* vol 3 (United States: ASM International)

[10] Hall D E 1983 *Plat. Surf. Fin.* **70** 59

[11] Bruet H, Bonino J P and Rousset A 1999 *J. Matter. Sci.* **34** 881

[12] Anwar S, Khan F and Zhang Y 2020 *Process Saf. Environ. Prot.* **141** 366

[13] Bhat R S and Shet V B 2020 *Surf. Eng.* **36** 429

[14] Qiao G, Jing T, Wang N, Gao Y, Zhao X, Zhou J *et al* 2005 *Electrochim. Acta.* **51** 85

[15] Idris J, Christian C and Gaius E 2013 *J. Nanomater.* **2013** 1

[16] Kim S-H, Sohn H-J, Joo Y-C, Kim Y-W, Yim T-H, Lee H-Y *et al* 2005 *Surf. Coat. Technol.* **199** 43

[17] De Vogelaere M, Sommer V, Springborn H and Michelsen-Mohammadein U 2001 *Electrochim. Acta* **47** 109

[18] Anwar S, Zhang Y and Khan F 2018 *RSC Adv.* **8** 28861

[19] Ciszewski A, Posluszny S, Milczarek G and Baraniak M 2004 *Surf. Coat. Technol.* **183** 127

[20] Kolonits T, Jenei P, Péter L, Bakonyi I, Czigány Z and Gubicza J 2018 *Surf. Coat. Technol.* **349** 611

[21] Abd El Rehim S and Ibrahim M 1998 *J. Metall.* **52** 34

[22] Kawano S, Ohgai T, Kobayashi S, Nakano H, Tsuru T, Akiyama T *et al* 2020 *Proceedings of the Second International Conference on Processing Materials for Properties* p 769

[23] Abd El Rehim S S, Fouad E E, Abd El Wahab S M and Hassan H H 1996 *Electrochim Acta* **41** 1413

[24] Nam D-H, Hong K-S, Kim J-S, Lee J-L, Kim G-E and Kwon H-S 2014 *Surf. Coat. Technol.* **248** 30

[25] Rashidi A and Amadeh A 2009 *Surf. Coat. Technol.* **204** 353

[26] Wasekar N P, Haridoss P, Seshadri S and Sundararajan G 2016 *Surf. Coat. Technol.* **291** 130

[27] Nakamura Y, Kaneko N, Watanabe M and Nezu H 1994 *J. Appl. Electrochem.* **24** 227

[28] Lotfi N, Aliofkhazraei M, Rahmani H and Barati Darband G 2018 *Prot. Met. Phys. Chem. Surf.* **54** 1102

[29] Brooks I and Erb U 2001 *Scr. Mater.* **44** 853

[30] Shibuya A, Kurimoto T, Hoboh Y and Usuki N 1983 *Trans. Iron Steel Inst. Jpn.* **23** 923

[31] Winand R 1994 *Electrochim. Acta* **39** 1091

[32] Inoguchi S, Kitada A, Fukami K and Murase K 2020 *J. Electrochem. Soc.* **167** 162511